THE UNIVERSITY of ADELAIDE

Using Spectral Induced Polarisation for water detection:

An example from the Mound Springs, South Australia.

Anastasia Costopoulos

Supervisor : Graham Heinson

Secondary supervisor: Michael Hatch

Abstract

Inland Australia is characterised by low rainfall and high evaporation rates making the knowledge about the location and quality of groundwater very important. The Great Artesian Basin (GAB) covers approximately 25% of Australia, and is central Australia's major source of groundwater, thus making it the most important source of water for this region. The springs of interest for the purpose of this study are located along the South-western margin of the basin within the Wabma Kadarbu Mound Springs Conservation Park. Our aim is to further our understanding of the spring systems within the GAB.

Groundwater and near surface geophysical surveys were used to develop parameters and state variables that aid in characterising near surface groundwater systems. Most electrical geophysical surveys designed to characterise hydrological problems measure only resistivity. This study employs the complex resistivity or Spectral Induced Polarisation (SIP) method as it provides the complete set of IP and resistivity data over a large range of frequencies and is therefore considered to be an added dimension to galvanic measurements.

There is a growing body of literature suggesting that the imaginary component of the IP and SIP response has a direct relationship with the hydraulic conductivity, however these studies have been carried out in controlled lab conditions. A major focus of this project is therefore to see if SIP can be used on a larger scale (i.e. field scale). As IP and SIP may be useful, there are several significant problems that have limited its success, with the key issue being contamination of data by electromagnetic (EM) coupling. Two attempts were made to evaluate and decouple the SIP data collected for this survey. The first was the residual analysis method and the second is based on the paper published by Pelton (1978). Our data analysis suggests that the EM coupling parameters are being resolved well. IP parameters however, require further investigation.

Key words: Great Artesian Basin, Induced Polarisation, Spectral Induced Polarisation, Electromagnetic Coupling

Contents

1.0 Introduction

Inland Australia is characterised by low rainfall and high evaporation rates making the knowledge about the location and quality of groundwater very important. The Great Artesian Basin (GAB) is central Australia's major source of groundwater, that covers approximately 25 % of Australia, across parts of New South Wales, Queensland, Northern Territory and South Australia (Figure 1) thus, making it one of the most important source of water for these regions (Welsh et al. 2005). The total capacity of the basin is thought to be around 8.7 X 10^9ML (Habermehl 1980). The basin is comprised of a multi-layered aquifer system, with aquifers developing in quartzose sandstones (most likely of continental origin) and separated by impervious beds of siltstone, mudstone and marine sediments of Middle Triassic to Late Cretaceous age (Habermehl 1980).

The springs of interest for the purpose of this study are located along the South-western margin of the basin within the Wabma Kadarbu Mound Springs Conservation Park (Figure 1). The systems that control the springs have been extensively investigated, but as the system is complicated, little is known of their deep structure. In this project the University of Adelaide group has used electrical geophysical techniques to try to help define the fluid pathways that feed the mound springs and the movement of groundwater in the GAB. These include induced polarisation (IP), magnetotellurics (MT), transient electromagnetics (TEM) and self potential (SP). This thesis focuses on producing a characteristic signature of the Mound Springs using resistivity and induced polarization (IP) techniques. It is hoped that as a result of this survey the data obtain can be further used to understand their structure, formation, possible changes in their hydrological regime and possible means for sustaining them.

Groundwater and near surface geophysical surveys are being used to develop parameters and state variables that facilitate in characterising near surface groundwater systems. The use of geophysics for groundwater studies have arisen as a means to reduce environmental damage and costs associated with

bore drilling. For groundwater studies resistivity surveys are used for relating the electrical current that flows through a medium to the applied electrical field (Kirsch 2009).

Most electrical surveys used to characterise hydrological systems have used resistivity and or high resolution TEM. Figure 2 illustrates one example of a TEM survey over another GAB mound spring system. IP (specifically Spectral IP) has not been tested over these systems before. The purpose of this study was to run a resistivity and IP survey over the spring system to see if the IP/SIP component could provide additional information to be worth the extra effort. It should be noted that this survey required approximately three days to complete one 800m line, whereas a survey measuring just resistivity would use much shorter spacings (and therefore have higher resolution) and would require at most half the time to complete

There is a growing body of literature suggesting that the imaginary component of the IP and SIP response has a direct relationship with the hydraulic conductivity, however these studies have been carried out in controlled lab conditions. A major focus of this project is therefore to see if SIP can be used on a larger scale (i.e. field scale).

As useful as IP and SIP may be, there are several significant problems that have limited its success, with the key issue being the data acquired are often contaminated by electromagnetic (EM) coupling due to array geometry and geological layering (Zonge K 1981). Resistivity anomalies produced in the data are likely to come from chargeable features in the area such as shales and sulphide mineralisation. Other resistivity variations are controlled by the presence of fluids, where it is believed that the main aquifers and springs will have higher resistivity values due to the flow of relatively fresh water. When comparing this to the subsurface surrounding the springs, it is likely to be found that this area may be more conductive due to the presence of saline waters as it contains ionic (chargeable) particles that are trapped within the surrounding clay rich rock. IP anomalies are a little hard to define as the contamination of EM coupling reduces the validity of measured anomalies in the data.

2.0 Background

2.1 Hydrogeology of the Great Artesian Basin

The GAB is a confined groundwater basin which in turn is comprised of three sedimentary sub-basins: the Eromanga, Surat, and the Carpentaria (Figure 3a) as well as the upper parts of the Bowden and Galilee basin (Habermehl 1980). The three major basins range from Cretaceous to Jurassic in age and are characterised by sediments that have a low to very low permeability (Habermehl 1980). Overall the GAB is an asymmetrical basin which elongates towards the north-east - south-west, tilting towards the south-west. Uplift along the eastern margin of the Great Dividing Range occurred during the Late Cretaceous to Early Cainozoic. Subsidence occurred also during this period along the south-west margin, resulting in the basins characteristic asymmetry (Cox. 1998). Major fault and fold systems have formed across the whole basin, but do not have a broad scale effect on the regional hydrogeological patterns (Keane 1997). Although there is no regional effect of active geological movement many near surface folds appear to grade downwards into fault systems forming echelon structures (Cox. 1998).

The aquifers are well separated from the salinity waters of the Permian units of the basin, except in the south west region where Permian-Triassic strata are in direct contact with Jurassic aquifers (which have a high salinity) (Habermehl 1980). Models of the groundwater flow simulated by Habermehl (2001) suggest that the majority of the water enters the basin through areas where the sandstone formations are exposed or buried beneath highly porous sand sheets along the margins of the basin (Fensham and Fairfax 2003). The groundwater flow patterns are quite complex but as previously mentioned the general direction of water flow is towards the south-western margin. Along the eastern margin of the basin some outcropping sediments are known to be 1000m above sea level, whilst the ground surface along south western margin approaches near sea level (Fensham and Fairfax 2003). The hydraulic head or potentiometric surface of the basin aquifers are determined by the elevations of the recharge areas. Studies by Habermehl (1980, 2001) found that the hydraulic head decreases away from recharge areas, as water pressure is lost when it permeates through aquifer

sediments. Further reduction of the water pressure within the basin has resulted from the development of artesian water bores (Fensham and Fairfax 2003, Habermehl 1980).

The GAB is composed of a series of transgressional alluvial, fluvial and marine sequences deposited during the Neoprotoezoic era, with deformation occurring during the Jurassic and Cretaceous periods (Keppel et al.) The main aquifer in South Australia is comprised of sand, silt and gravel of the Algebuckina sandstone and the Cadna-Owie Formation (Department of Water Resources 2000). The Algebuckina Sandstone (which underlies Cadna-Owie Formation) has a maximum thickness of 750 m whilst the Cadna-Owie Formation is typically 20 to 40 m thick around the basin margin and up to 100 m thick in the deeper parts (Department of Water Resources 2000). The Bulldog Shale overlays the Cadna-Owie Formation and forms a partially effective confining bed (Department of Water Resources 2000). The aquifer units within the GAB significant to the study include the Cadna-Owie Formation and the Bulldog Shale with a detailed description of these sites provided in section 2.4.

The central part of the basin is up to 3,000m thick (Figure 3) and is estimated to contain up to 64,900 cubic kilometers of groundwater. The majority of the recharge to the aquifers occurs from relatively higher ground on the western slopes of the Great Dividing Range (Baker 2007), to the western margin, where water is up taken through the pores between the sand grains (Cox. 1998). Groundwater flows mainly westward towards the southwest and to the north and northwest in the northern part of the basin at around 1 to 5 m per year The total discharge of the GAB is estimated at 1096 ML/day, much of which occurs as natural discharge in the form of outflow and as seepage from springs (mostly in the southern part of the basin). The age of the groundwater, determined from a combination of hydraulic modelling and carbon-14 and chlorine-36 studies ranges from several thousand years for the recharge areas in the north to nearly 2 million years in the south-western discharge regions (Mudd 2000).

2.2 Hydrochemistry of the Great Artesian Basin Groundwater

The hydrogeochemistry of the GAB groundwater is dominated by sodium bicarbonate ($NaHCO_3$) with traces of chlorides and sulfides (Mudd 2000). The $NaHCO_3$ ions accounts for approximately 90% of the total dissolved salts in the basin (Mudd 2000). The remaining 10% is dominated by sodium sulfides (Na_2SO_4) and is present in the western and south-western region of the basin.

Recharge areas contain a higher proportion of calcium, magnesium and sulfate ions, which decreases basinwards (Habermehl 2001). In the centre region of the basin, the concentration of chloride ions appear to increase and the concentration of the dissolved oxygen decreases. The semi – stagnant flow of the water here may be accountable for the high concentrations of ionic compounds as there is less internal mixing of the water

The Lower Cretaceous to Jurassic aquifers generally have lower salinities than its Cretaceous counterparts (Habermehl 2001). The quality of groundwater improves with increasing depth within the aquifers of the Lower Cretaceous to Jurassic sequences, which was discovered from samples of water attained from the aquifers. The results indicate that the groundwater alkalinity levels are lower in comparison to the aquifers within the Cretaceous sequences and the concentration of total dissolves salts appear to be significantly reduced (Habermehl 2001).

2.3 Mound Springs

A classic mound consists of a central pool of water with an outer rim of salt tolerant reeds and other vegetation, an outer flow channel and successive layers of carbonate as illustrated in Figure 4a. The conical mounds (which are characteristic of these springs) are formed by the accumulation and cementation of carbonates, sand, silt and clay. An important feature of their construction is the escape of water from the confined aquifers along fault lines, shattered rock and the accumulation of porous sediments in and around the mounds (Williams and Holmes, 1978) as illustrated in Figure 4b.

Active and extinct artesian spring mounds are distinct features present in the basin and have found to be associated with local and regional geology such as faults and fault zones (Ponder 1986). Additionally some are hypothesised to have developed as a result of erosion of the confining beds (Cox. 1998). There are at least 11 main groups of springs that occur in the lower GAB, as indicated in Figure 3b, where their location represents either isolated discharge points or areas of discharge where groups of springs have amalgamated (Ponder 1986, Habermehl 1982)

The overall outflow from the springs is roughly 137 ML per day, 62% of which is from South Australian springs (Harris 1992). Harris (2001) states that it is likely that there are more than 600 vents in the south-eastern corner of the GAB, ranging from minor seepages at the base of hills, to others consisting of large pools of water. The oldest springs are extinct Pleistocene mounds, like the Hamilton Hill complex, which is located in the survey area studied for this project, i.e. Wabma Kardarbu National Park. These extinct springs reflect conditions when the GAB had a much higher hydrostatic head than at present (Cox. 1998).

The importance of the natural and cultural heritage associated with the springs has been well established in South Australia. The springs are the only permanent source of water in the arid interior of South Australia making them an important refuge for wildlife during drought conditions (Mudd 2000).

2.4 Geology of study area

Wabma Kadarbu Mound Springs Conservation Park covers an area of approximately 1,000 hectares and is located in central South Australia, approximately 750km from Adelaide.

The main aquifer units significant to this study include a yellow brown, calcitic, fine to medium sandstone known as the Cadna-Owie Formation and a medium to dark brown grey silty to fine sandy mudstone with lenticular laminate of pale to medium micacious silt known as the Bulldog Shale. The Bulldog Shale overlays the Cadna-owie Formation and forms a partially effective confining bed (SA Department of Water Resources 2000). The Algebuckina Sandstone underlies Cadna-owie Formation

and has noteworthy properties as a water reservoir but is too far down within the basin for it to be significant for this study. The area is overlain by surface alluvial deposits, including quaternary age fine quartz sandstones and brown gypsiferous sand. The surface drainage for the study area is predominantly to the east toward Lake Eyre South. The topography of the region is relatively flat with variations commonly provided by sand dunes(1-5m height), drainage channel openings and extinct mound springs (SA Department of Water Resources 2000).

3.0 Methods

3.1 IP theory

Most electrical geophysical surveys designed to characterise hydrological problems measure only resistivity. This study employs the complex resistivity or SIP method as it provides the complete set of IP and resistivity data over a large range of frequencies and is therefore considered to be an added dimension to galvanic measurements.

According to Börner and Schön (1995) conductivity changes with frequency and therefore can be expressed as:

$$\sigma(\omega) = \sigma'(\omega) - \mathrm{i}\sigma''(\omega) \qquad (1)$$

Which defines σ' as the real component, $\mathrm{i}\sigma''$ as the imaginary component and ω as the angular frequency (Börner and Schön 1995). What is measured from equation (1) is usually the resistivity (i.e. the inverse of conductivity) and phase shift at each frequency. Characterising how phase and resistivity change with frequency has been shown to correlate with important information about the subsurface (Pelton et al. 1978, Zonge K 1981) and is an area of ongoing research.

EM coupling can be defined as the inductive response of the Earth, which manifests itself as a response over the induced IP signal (Routh and Oldenburg 2001) and is a major obstacle to the interpretation of IP and SIP data (Wait 1986, Wynn 1977). EM coupling is directly proportional and highly influenced by at least four factors. These include: dipole length, distance between the transmitting and receiving electrodes, conductivity and frequency (Hatch 2011).

3.2 Data Acquisition

IP data were collected across a single line, in the south-east corner of the Wabma Kadarbu Mound Springs Conservation Park, 800m in length (Figure 5). Data were collected at 25 m dipole-dipole spacing using a Zonge multipurpose GDP-32 II receiver and a Zonge GGT 10 transmitter with electrode separations from n=1 to 6. The receiver is microprocessor controlled and capable of simultaneously collecting data on up to sixteen channels controlling signal frequency and synchronisation (Zonge K 1981). A minimum of 3 readings were collected at each station and were averaged out, producing a single data point for each station. Data collected were backed up daily from the receiver memory.

A linear distribution of 29 transmitting electrodes were used, each connected to the transmitter. Transmitter electrodes were made out of two to five stainless steel rods that were driven into the ground. When in areas of solid rock, heavy-duty aluminium foil pits were built and put into place.

The resistivity and phase were measured using fundamental frequencies of 0.125Hz, 1Hz and 8Hz; and their first 5 odd harmonics. That is, if the frequency is measured is 0.125Hz the data obtained will be at 0.125Hz plus the next 4 odd harmonics, i.e. 0.375, 0.625, 0.875, and 1.125 Hz. As SIP provides the most complete set of IP data the use of a 1Hz fundamental and the harmonics of 3, 5, 7 and 9Hz are produced as well as an 8Hz fundamental with the harmonics measuring at 24, 40, 56, and 72Hz (Zonge K 2005, Zonge K 1981). A periodic square wave function was used in this survey and

is expressed in Figure6. Figure 6 is a fourier transform that illustrates the first 5 harmonics and their summed approximation of the square wave (Zonge K 1981).

3.3 Data Processing

3.3.1 IP and Resistivity

The data were initially processed and inverted using Zonge's TS2DIP inversion program which is based on a 2D smooth model inversion. Prior to inversion a 3-point decoupling removal algorithm was employed (using the Zonge GDP receiver) in order to reduce the EM coupling effect. This algorithm assumes that the SIP effect at low frequencies is independent of the EM coupling effect (Zonge 1981) which is effectively 0Hz IP effect. The inversion model converts apparent resistivity and phase vs n-spacings into real resistivity and phase vs depth as seen in Figure 7a and 7b. Topographic information is incorporated to produce elevation features. Inversion results are then output into tabular ASCII files and then plotted as sections.

3.3.2 Spectral IP

Two attempts were made to evaluate and decouple the SIP data collected for this survey. The first was the residual analysis method and the second is based on the paper published by Pelton (1978). Both will be described here.

There have been a number of approaches at decoupling IP data, including by Pelton(1978), Zonge(1981), and Bin-Xiong (2006). All are based on equations such as the Cole-Cole equation, but are quite complicated and difficult to implement. The paper published by Pelton (1978) has gained wide recognition for decoupling IP data in characterising an IP response by fitting curves in a real and imaginary space using a mathematical model, as expressed below.

$$Z = R(0)\left[1 - m_1\left(1 - \frac{1}{1 + (j\omega\tau_1)c_1}\right) + m_2\left(1 - \frac{1}{1 + (j\omega\tau_2)c_2}\right)\right] \quad (2)$$

(Xiang et al. 2002)

From equation (2) Pelton (1978) demonstrates how a simple view of mineralised rock results in a relaxation model containing four parameters that matches any curve in the real and imaginary space. Using equation (2) the parameters with a subscript of 1 (m_1, tau_1, c_1) are the IP effect and the parameters with a subscript of 2 (m_2, tau_2, c_2) are EM coupling. (Units m_1 and m_2: ratio of voltage immediately after to voltage immediately before current is stoped, units of tau_1 and tau_2: seconds).

The first technique used in an attempt to decouple the full data set is known as the residual analysis method. This was a first pass attempt to provide any evidence about how the ground response changes across the system. The second technique employs equation (2) from Pelton (1978) where a directed Monte Carlo simulation was to randomly sample the data using equation (2) in order to process its results.

Figure 8 shows coupled EM and IP response for all the n-spacing's (n1-6). At the scale that they are plotted at all the responses look the same, but in reality they are not i.e vary at fine scales. For that reason the EM coupling effect is what is being observed plus ground response.

The logic is that the EM coupling at any n value will be quite small across the array. Therefore if that the end readings are taken (e.g n=6) and subtracted from all the other values something systematic will develop in the data set, similarly for n=5 subtract the end station from all of the others. This is known as residual analysis, where the remaining data will be analysed to determine the SIP response. This was the initial step to see what the first response looked like, the end station was chosen as this is where most of the coupling is supposed to have occurred and then subtract it from its self and then from every other station. The assumption is that the end responses are background(away from the spring system), consequently the remaining data (once the background is

removed) is the part of interest. Figure 9a and 9b show two n –spacing results (n=3 and n=5) from the residual analysis technique.

The directed Monte Carlo approach was used to decouple SIP data using equation 2 (Pelton 1978). This procedure was carried out twice, the first time the parameters m_1 and m_2 and tau $_1$ and tau_2 were allowed to vary over a wide range. The second run focused on narrowing down the range that m_2 and tau_2 were allowed to vary. Using equation (2) values for RØ, c_1, c_2, m_1, m_2, tau_1 and tau_2 were investigated. As specified in Pelton (1978) c1 and c2 were set to 0.25 and 1 respectively. Limits were set for RØ to vary from the 0.125Hz resistivity ($\pm$ 1 Ωm) that was collected whilst in field. As suggested in Pelton (1978) m_1, and m_2 were let to vary from 0 to 3 (Units: ratio of voltage immediately after to voltage immediately before current is stopped (Pelton et al. 1978)) and tau1 and tau2 were allowed to vary from $1x10^{-8}$ to 1 seconds . This was set to run for each station for 1 million trials in its first run. After the first run it was determined that m_2 and tau_2 varied by n-spacing, thus they were adjusted so that they varied only from their mean at each n-spacing $\pm$ 2x the standard deviation. By doing this it was hoped that the values of m_1 and tau_1 (i.e. the ground response) could be narrowed down in another run of the Monte Carlo search routine.

4.0 Results

Results and pseudo sections were established around one line, south – east corner of the Wabma Kadarbu Mound Springs Conservation Park (Figure 5). This location was chosen as it contained two small spring systems and as data were able to be collected without using a vehicle to as this was untracked land.

4.1 Raw data

The inverted resistivity model (Figure 6a) represents a basic layering pattern that alternates from resistive at the sub- surface, which overlays a conductive features, that in turn overlays a

resistive feature. The IP inversion (Figure 6b) highlights a strong response between stations 5125 and 5175. Within this figure distinguishable structural features in the landscape are apparent.

4.2 Residual analysis

Figures 9a and 9b have been generated from the residual analysis technique and were developed in order to separate the EM coupling effects from the ground response. In the real component there is a broad region where the residual is positive and a broad region where the residual is negative. For the imaginary component it appears that the response is the opposite way around from the real residual (i.e. where there is a positive response in the real component, there is a negative response in the imaginary component). The responses from the real component do not amplify any features in the area in comparison to the imaginary component. From the figures it appears that as the n-spacing increases the EM coupling may still be overwhelming the ground and IP response. In all (n=1 to n=6) of the imaginary component responses there is a notable point where the response changes dramatically from negative to positive suggesting that there is a change in the response of the earth. The main findings in the imaginary residuals are seen at the higher frequencies (9 to 72Hz). Thus it can be inferred that that the response of the system at the northern end of the line (end stations) may have different coupling than in other places and that the ground response is more strongly pronounced at 72 hertz. From examining these figures it is apparent that the IP effect is at its strongest between stations 5300 and 5450.

The amplitude response from the residual analysis illustrates that it increases from the south end of the line to the north end of this line as illustrated in Figure 10ai and 10aii. When looking at the phase responses (n=1 to n=6) in most parts it appears rather consistent, that is, the pattern in which it exhibits is consistent though all the n-spacings. In Figure 10bi and 10bii the phase response appears to loop around, i.e. response is going beyond 180 degrees and rather than the response being displayed as 181 degrees, its represented as negative 179 degrees, creating a discontinuity in the data plot. The frequencies between 9Hzand 24Hz appear to be grouped together quite tightly, as with the

frequencies between 40Hz and 75Hz. There was little change in the amplitude and phase with the lower frequencies therefore were not used since the higher frequencies show the strongest responses.

4.3 Directed Monte Carlo approach to decoupling IP data

Figure 11 shows argand diagrams that illustrate the relationship between the coupled response and the ground response. Figure 12, shows scatter plots that compare resolution of parameters in the best 1% of Monte Carlo results for one site.

Figures 11i to 11vi illustrate how the coupled data varies from the decoupled data along the line. These figures show the results for the n-spacing of n = 4 as it is likely to have a less coupling than the subsequent n-spacings of 5 and 6, yet is not influenced by noise from the subsurface of n-spacings 1, 2, and 3. Figure 11bi to 11bii show the relationship between the coupled response and the ground response when the n-spacing is increased.

Figure 12, shows scatter plots that compare the resolution of parameters in the best 1% of Monte Carlo results. The parameters m_1, m2, tau_1 are plotted against each other as illustrated in Figure12. Within each of these plots it is apparent that many of that data points do not fit the data, yet these plot show the 1% best fit thus how well the data has been decoupled needs to be considered. Figure 12a showing m_1 against m_2 (ground response against EM coupling) illustrates that both parameters cluster close together towards lower values, yet m_2 is never less than 0.25, but m_1 can vary from 0 to 3. Figure 12b presents the comparison between m_2 and log of tau_1. In this figure m_2 varies between 0.25 and potentially greater than 3. The log of tau_1 on the other hand varies widely but tends to cluster together around the lower range. Figure 12c shows the relationship between m_1 (ground effect) and log tau_2 (EM coupling). This figure shows some correlations between the two parameters in that the data plotted within a narrow range. Log tau_2 in particular occurs within a limited range of log -3 to log -2, whereas m_1 tends to localise within the lower regions. Figure 12d is highly correlated as it

exhibits the relationship between the two coupling parameters m2 and log tau_2. Log tau_2 in this figure shows that it occurs within a limited range, whereas m_2 can vary from less than 0.25 to potentially greater than 3. Figure 12e illustrates the plot of m_2 against tau1 and shows that there is a link. In this figure m_1 values can be high or low and contrast with tau_1 values (i.e. when m_1 is low tau_1 is low), suggesting that this scatter plot shows some strong correlations.

5.0 Discussion

Preliminary interpretations of the resistivity inversion (Figure 6a) indicates that there is a region of higher resistivity possibly due to a moderately dry surface layer that overlies a low resistive layer which is thought to be the Bulldog shale (roughly 25m thick). A small indication of the next resistive layer is picked up in this inversion, which could possibly the Cadna-Owie formation (main aquifer of the GAB). The presence of conductive fluids (recharge) could be another explanation for the relatively higher electrical conductivity. IP inversion (Figure 6b) shows its biggest effect around 5150. Structural features in the landscape emerge in Figure 6b and may indicate that there may be some vertical movement of fluid in the spring system. Another explanation for this anomaly is that a fault may have been cross-cut, resulting in the alteration and brecciation of the highly chargeable Bulldog Shale.

The residual analysis technique was used a first pass filter to determine how much coupling there is at each frequency by subtracting the end station from the subsequent readings to see any change in the responses. Variations along the line do not seem to show much of an influence with the known location of the spring. Some variations at the end of the line (more specifically the northern end) appear to coincide with the location of the highly conductive surface waters and salt precipitation on the ground surface. A varying trend emerges in all of the real and imaginary residual plots and is characterise by a strong negative response in the imaginary component. The assumption for this response is that it is a drainage channel that facilitates fluid pathways, but does not appear to have a direct correlation to a spring system.

Amplitude results (Figure 10ai and 10aii) indicate an increase from the southern end of the line to northern end. From studying the phase responses a likely reason for the results looping around is due to the subtraction of the residual, thus the plots scatter around the same point but in different locations within the quadrant. This results in both positive and negative readings. For a large number of data points the phase is consistently different, but when looking at the lower frequencies (8-24Hz) the phase is more scattered and therefore loops around. From once the points start scattering any kind of real knowledge of what happening is lost and it is less obvious what exactly is happing in the system.

To further narrow down and improve the understanding of the spring system, pseudo sections of the highest frequency response were produced, i.e. 72 hertz. The higher frequency end provided the strongest response in the residual analysis method acting as an envelope to the SIP response, as response at lower frequencies is generally less than at 72 hz. Figure 13 illustrates the real, imaginary, magnitude and phase responses at 72Hz at all 6 n-spacings. There are small variations throughout the real, imaginary and magnitude responses, but does show some changes in conductivity towards the end of the line. The phase (Figure 13d) shows a great deal of sign variation, which makes it easier to distinguish patterns. The location point between the red and blue colours indicates that the phase is wrapping around between positive and negative 180. Between stations 5300 – 5400 there is a wide feature at the surface, with n=1 showing the strongest response and narrows at depth. It appears that the feature is narrowing with depth and that fluid is moving in a vertical movement towards the surface. However the shape of an anomaly in a pseudo section can be quite different to what it converts to in an inversion therefore conclusive outcomes cannot be made.

From carrying out the residual analysis technique there are potentially two possible explanations causing these results:

1) The chargeability varies across a smaller scale; therefore the 25m station spacing used may have been too coarse to pick up the finer features that were expected at Wabma Kadarbu.

2) There are two possible sources for chargeability in this area, one souce could be due to the presence of clays within the subsurface. The other source could be as a result of sulfidic materials. These two ionic species could reduce validity of the results as EM coupling is influenced by ionic materials and therefore is dominating over the IP response.

Wabma Kadarbu Mound Springs Conservation Park happens to be more conductive than the survey carried out at the Warburton and Beresford springs. This was determined by comparing the resistivity data (Figure 6a) with the high resolution TEM data (Figure 2). The resistivity inversion shows the basic story of the area but it does not have the resolution that the TEM data shows. Laterally the figures are similar as they are on a similar scale. Low resistivity features along the flanks are apparent in both figures. This could be the Bulldog Shale that that both methods are picking up. Vertically the results are quite different, the high resolution TEM data is of a higher resolution and its features are well distinguishable due to a smaller field and smaller spacing. Another explanation for the higher conductivity in the Wabma Kadarbu area is that there could be more subsurface discharge that is evaporating. This discharge occurs through the fluid pathways towards the subsurface outlets, resulting in water accumulating on the subsurface which then evaporates causing salt precipitation to form on the surface.

The Pelton (1978) approach used to decouple the data proves to be useful in the respect that it has (to a degree) separated out the EM coupling from the ground response. Argand diagrams represented in Figure 11 show slight changes in the strength of the ground response as the distance between the transmitting and receiving electrodes increase. This is represented by changes in the angle between the ground response and the EM coupling response. Focusing in on this change in angle is greater defined, yet it does not show any conclusive results of the relationship between the EM response and the decoupled ground response. Two likely explanations can be made from this:

1) There is minimal to no IP effect/ response in the area, as a result the responses don't give any real indication of what is happening;

2) From the using equation (2) to decouple the data the limits set to remove the coupling may be too wide, therefore may not be removing enough of the coupling and thus are still finding it difficult picking out subtle differences in ground SIP response.

The scatter plots in Figure 12 are a result of a random sampling technique using equation (2) posed by Pelton(1978) and indicate how pairs of the parameters are linked. The Monte Carlo inversion simply finds sets of models that fit the data to some level of quality. There is an absolute best fit (in the least squares sense) but there are also a range of models that fit the data reasonably well. What these plots show are the scatter of acceptable models and how they are linked. For example, in the plot of m_2 against tau_2(Figure 12d) , the value of tau_2 for all models lies between -2 and -3 on a log scale; however, m_1 is much less well constrained, and can, depending on other parameters, be anything between 0.5 and greater than 3. In the plot of m_1 against m_2, there is little correlation (that is, they are quite independent). The plot of m_1 against tau_1 (Figure 12e) shows there is a link, and can either have high m_1 values (and low tau_1), or low m_1 values (and high tau_1). In other words, two scatter plots (m_1 against log tau_2 and m_2 against log tau_2) are strongly correlated and the remainder plots show a negative correlation. The range of m_1 and m_2 should be greater than 3 as it appears that the points go beyond that range. There are small limitations in the range in which tau_2 can vary however tau_1 tends to be small but its range should be extended to less than $1x10^{-8.0}$. In general, if the points are all clustered close together, then parameters are well resolved. If they are vey spread out, then there is little correlation and the parameters are poorly constrained. This simulation conveys to people about the confidence of these parameters and what this tell us about the coupling co-efficients.

The final section involved producing pseudo sections (Figure 14) to express what these scatter plots mean. M_2 shows more uniform values, and given that each value is completely independent at a

Monte Carlo measurement there is a lot of confidence that what the figures are a true value of measurement of what is seen in the field. The standard deviation was determine to be 1.5, when comparing this to the scale on the colour the errors are much smaller than what is in the shown on the scale, therefore have a lot of confidence that they are an accurate value of measurement. Tau_2 is expressed on a log scale and again is quite uniform with only a small amount of variability at the top. As a result the coupling is actually quite uniform in these arrays. In terms of m_1 (IP effect) (0.4 is the average standard deviation) the error bar is with the blue region of the colour bar and is determined quite well. The Monte Carlo simulation shows that the EM coupling is quite uniform and an increase with depth i.e. gets bigger with n-spacing but not a huge amount of variation is show. In the IP response – tau_1 is appears to be below the noise level, from equation (2) if tau1 is really small it means that the entire term on the bottom is really small and therefore has no real effect at all. The standard deviation for m_1 is 0.4 consequently the plots that are likely to how any try value of measurement are below this point, thus is seen in n=1 between the first few points.

6.0 Conclusion

The concept with the residual analysis technique was to use a simple method to at least separate out most of the EM coupling from the ground response in the data. From this technique final outcomes made include;

1) EM coupling is still present in the responses. This might be due to the fact that the resistivity varies across the area, i.e. the EM coupling and frequency response changes at each site. Might say that across this area there is something different south of the line than there is north of the line and that could be because the geology is different.

2) EM coupling effect (although still present) may be small; therefore the changes could be due to the IP effect.

The decoupling technique from Pelton (1978) may not be that proficient as the n=1 in the data set appears to be disproportionally bigger compared to the subsequent n-spacings. This indicates that the EM coupling parameters are being resolving well, but not so well the IP parameters. This is perhaps because they are smaller than the EM parts, and more dominated by noise.

A full comprehension of the connectivity between the stream recharge and groundwater table conductive features is not well understood, making it hard to correlate and postulate whether these anomalies identified are useful in improving our knowledge of hydrological structure in this area. Inductive EM coupling plays a major role in the validity of the data. A repeat survey possibly with smaller electrode spacing may improve resolution enough to fully identify the finer scale surface features like the Bulldog Shale and expand on the understanding of the groundwater distribution.

7.0 Acknowledgments

I would like to thank my supervisor Dr Graham Heinson and my associate supervisor Michael Hatch for their enormous contributions guidance and support throughout this year, without their knowledge and assistance, this study would not have been successful. I would also like to thank Kent Inverarity for his keen assistance with our field work.

Special thanks also to this year's class, especially those in room G10 for their invaluable assistance. Not forgetting my outside university friends who always been there. I would also like to express gratitude to my family for their understanding & love, through the duration of this thesis.

I like to convey thanks to the National Water Commission for providing the financial means to this study.

8.0 References

Baker P. 2007. Science for Decision Makers: Groundwater recharge. *Australian Bureau of Agricultural and Resource Economics and Sciences*, 1-8.

Börner, F.D. & Schön, J.H. 1995. Low frequency complex conductivity measurements of microcrack properties. *Surveys in Geophysics* **16**, 121-135.

Cox. R., A.B. 1998. Resource study - Chapter 1: Background to the GAB. *From GAB Coordinating Committee* **1**, 11-72.

Department of Water Resources, G.o.S.A. 2000. Water Resource Assessment: Great Artesian Basin - SA **Fact Sheet 10**, 1-4.

Fensham, R.J. & Fairfax, R.J. 2003. Spring wetlands of the Great Artesian Basin, Queensland, Australia. *Wetlands Ecology and Management* **11**, 343-362.

Habermehl. 2001. Hydrogeology and Environmental Geology of the Great Artesian Basin, Australia. *In: Gostin, V.A.(ed.), Gondwana to Greenhouse - Australian Environmental Geoscience - Australian Environmental Geoscience. Geological Society of Australia Inc., Special Publication* **Chapter 11**, 127-143, 344-346.

Habermehl, M.A. 1980. The Great Artesian Basin, Australia. *BMR Journal of Australian Geology & Geophysics* **5**, 9-38.

Habermehl, M.A. 1982. Springs in the Great Artesian Basin, Australia - their origin and nature. *Australian Bureau of Mineral Resources, Geology and Geophysics, Report* **235**.

Harris, C. 1992. Mound Springs: South Australian Conservation Initiatives. *The Rangeland Journal* **14**, 157-173.

Harris, C. 2001. Culture and geography: South Australia's mound springs as trade and communication routes,. *Paper presented at Australia ICOMOS 'Making Tracks' Conference May 2001.*

Hatch, M. 2011. Personal Communication

Keane , D. 1997. The Sustainability of use of groundwater from the south - western edge of the Great Artesian Basin, with porticular reference to the impoact on the mound springs of the borefields of Western Mining Corporation. . *Phd Thesis*, 1-68.

Keppel, M.N., Clarke, J.D.A., Halihan, T., Love, A.J. & Werner, A.D. Mound springs in the arid Lake Eyre South region of South Australia: A new depositional tufa model and its controls. *Sedimentary Geology*.

Kirsch, R. 2009. Groundwater Geophysics. *Groundwater Geophysics*, 227 - 252.

Mudd, G.M. 2000. Mound springs of the Great Artesian Basin in South Australia: a case study from Olympic Dam. *Environmental Geology* **39**, 463-476.

National Water Commission's Allocation. 2011. Water and Maintaining Springs in the Great Artesian 1-16.

Pelton, W.H., Ward, S.H., Hallof, P.G., Sill, W.R. & Nelson, P.H. 1978. MINERAL DISCRIMINATION AND REMOVAL OF INDUCTIVE COUPLING WITH MULTIFREQUENCY IP. *Geophysics* **43**, 588-609.

Ponder, W. 1986. Mound springs of the Great Artesian Basin. *Limnology in Australia: De Deckker P, Williams WD (eds)*, 403-420.

Routh, P.S. & Oldenburg, D.W. 2001. Electromagnetic coupling in frequency-domain induced polarization data: a method for removal. *Geophysical Journal International* **145**, 59-76.

Wait J.R., G.P. 1986. On electro magnetic coupling removal from
induced polarization surveys. *Geoexploration* **24**, 21-27.

Welsh, W., J., D., Institution, B.o.R.S.K.A. & Australia. 2005. Great Artesian Basin groundwater modelling.

Williams, A.F. & Holmes, J.W. 1978. A novel method of estimating the discharge of water from mound springs of the Great Artesian Basin, central Australia. *Journal of Hydrology* **38**, 263-272.

Wynn, J.C., Zonge,K.L. 1977. Electromagnetic coupling. *Geophysical Prospecting*, 29-51.

Xiang, J., Jones, N.B., Cheng, D. & Schlindwein, F.S. 2002. A new method to discriminate between a valid IP response and EM coupling effects. *Geophysical Prospecting* **50**, 565-576.

XIONG B, H.J., BAO L, FU G. 2006. A direct induced polarization decoupling scheme by chop wave. *School of Physics and Geomatics Engineering, Central South University*.

Zonge K, H.L. 1981. The Complex Resistivity Method. *in Advances in Induced Polarization and Complex Resistivity*, 163-203.

Zonge K, W.J., Urquhart S. 2005. Resistivity, Induced Polarization, and Complex Resistivity, Near-Surface Geophysics *Investigations in Geophysics; Society of Exploration Geophysicists* **13**, 265-299.

9.0 Figure captions

Figure 1: Location of Wabma Kadarbu Mound Springs Conservation Park and extent of the Great Artesian Basian, Australia. (Reproduced: Habermehl 2001)

Figure 2: TDEM resistivity section across Little Beresford spring (National Water Commission's Allocation 2011). This figure is of high resolution TDEM data that was collected on the Little Beresford spring, Beresford. Here . Data were collected at 20 m intervals using a 20 m by 20 m transmitting loop and a 5 m by 5 m receiving loop.

Figure 3a: The sub-basins of the Great Artesian Basin and the depth of their sediments (Cox. 1998). This figures illustrates the sedimentary sub-basins that make up the GAB, these include the Eromanga, Surat, and the Carpentaria. This figure was originally used by the Great Artesian Basin consultative council in their background report on the GAB.

Figure 3b: Spring supergroups of the Great Artesian Basin, represented by the dashed red lines. The grey shaded area represents the recharge zone (Reproduce (Fensham and Fairfax 2003). This figure shows the main groups of springs that occur in the GAB. The spring location specific to this study are within the Lake Eyre sub-group.

Figure 4a: Typical surface expression of a mound spring located at the Wabma Kadarbu Mound Springs Conservation Park in the survey area.

Figure 4b: Conceptual cross section of a mound spring. This Figure is an illustration from the paper published by (Williams and Holmes 1978) and amplify the important features of the spring construction, which include the escape of water from the confined aquifers along fault lines and shattered rock and the accumulation of sediments and precipitates in the mound itself.

Figure 5: Location and length of IP line at Wabma Kadarbu Mound Springs Conservation Park. This line funs in a south – north orientation, i.e. first readings were taken in the southern end and final reading was taken in northern end.

Figure 6: Inverted resistivity and IP data using the Zonge TS2DIP inversion program:

6a) showing resistivity inversion, resistivity calculated data and resistivity observed data. **6b)** Showing IP inversion, IP calculated data and IP observed data.

Figure 7: Graphic representation of Fourier synthesis of a square wave. This figure was used in Zonge (1981) for explaining the complex resistivity or spectral IP method. Zonge (1981) illustrates the first 6 odd harmonics and their approximation of the square wave. The wave coloured in red were the ones used in the project.

Figure 8: Argand diagrams illustrating responses over the whole frequency range.

Figure 8a): shows the SIP response at the northern end of the line for two n-spacings, n=3 and n=6. This figure demonstrates that EM Coupling has its strongest response here and does increase as n-spacing increases.

Figure 8b): Illustrates the complex resistivity path at the southern end for n=2 and n=5. Em coupling is still stronger at the larger n-spacing.

Figure 8c): Shows the SIP response midway down the line. N-spacing n=3 and n=6 illustrates that the EM coupling is clearer for the larger n-spacing.

Figure 9: Real and Imaginary plots from residual analysis method for n-spacings n = 3 and n=5.

Figure 9a): Shows the residual response for n = 3. This figure illustrates that the imaginary response soundly defines features in the landscape more effectively than the real component.

Figure 9b): This figure shows the residual response of the real and imaginary component for n=5. Here the landscape features are not as strongly defined in the imaginary component as they are for figure

Figure 10: amplitude and phase plots of the residual analysis data for n=3 and n=5.

Figure 10ai) and **10aii)** show the amplitude response over the system for both n=3 and n=5. Readings in figure 10 ai are grouped together more tightly than they are in figure 10aii. A likely reason for this is because as the n-spacing increases the results become more dominated by EM coupling.

Figure 10bi) and **10bii)** show the phase shift responses over the spring system. When comparing the two figures, figure 10bi shows a a more defined response in the phase shift that figure 10bii.

Figure 11: Illustrates argand diagrams showing the correlation between the coupled EM data and the decoupled ground data.

Figures 11i to 11vi illustrate how the coupled data varies from the decoupled data along the line.

Figure 11bi to 11bii show the relationship between the coupled response and the ground response when the n-spacing is increased.

Figure 12: Scatter plots formulated form random sampling using equation (2) suggested by Pelton (1978). These plots compare resolution of parameters in the best 1% of the Monte Carlo results. The range of figure 12a (m1 and m2)should be greater than 3 as it appears that the points go beyond that range. There are small limitations in the range in which tau 2 can vary however tau1 tends to be small but its range should be extended to less than $1x10^{-8}$. These figures tell you about the best fit chi squared and in reality there is a range of values that fit chi squared quite well. The other observation from these figures suggest how well correlated these are. In principle is if there is a high tau1 you would have a high tau2 and if tau2 were low, tau1 would also be low. In other words high tau2 cannot have a low tau1.

Figure 13: pseudo sections of real, imaginary, magnitude and phase response at 72Hz. Each pseudo section represented here is a representation of the response from the residual analysis technique. These pseudo sections are graphical interpretations of the of the highest frequency response which is 72 Hz.

Figure 14: pseudo sections of each parameter from data set posed by Pelton (1978)

This pseudo section illustrates the parameters derived from Pelton (1978) to visualise what the scatter plots (figure 12) look like and how well defined each limit is.

10. Figures

Figure 1

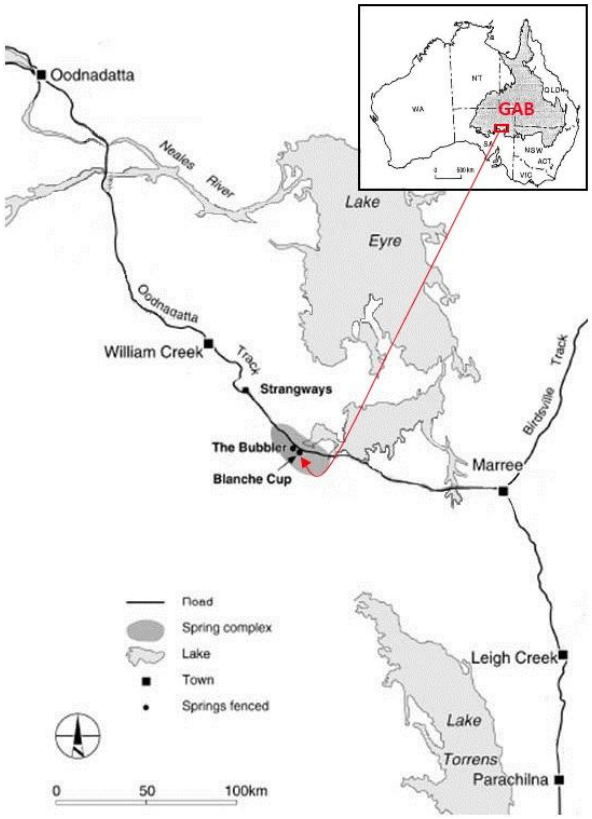

Figure 2

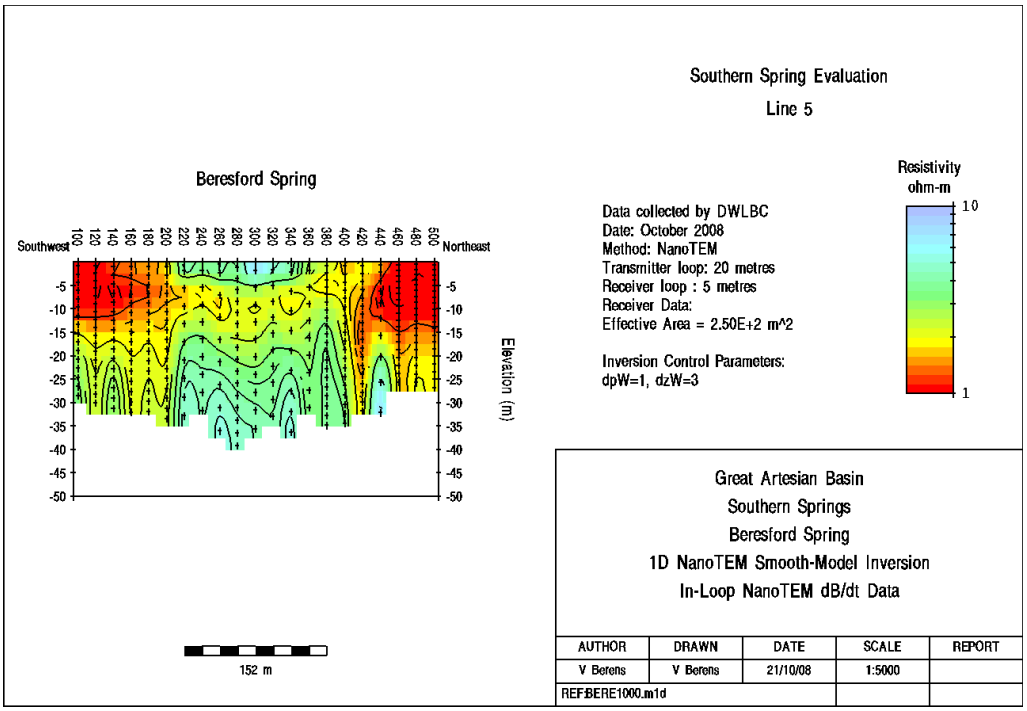

Figure 3a & 3b

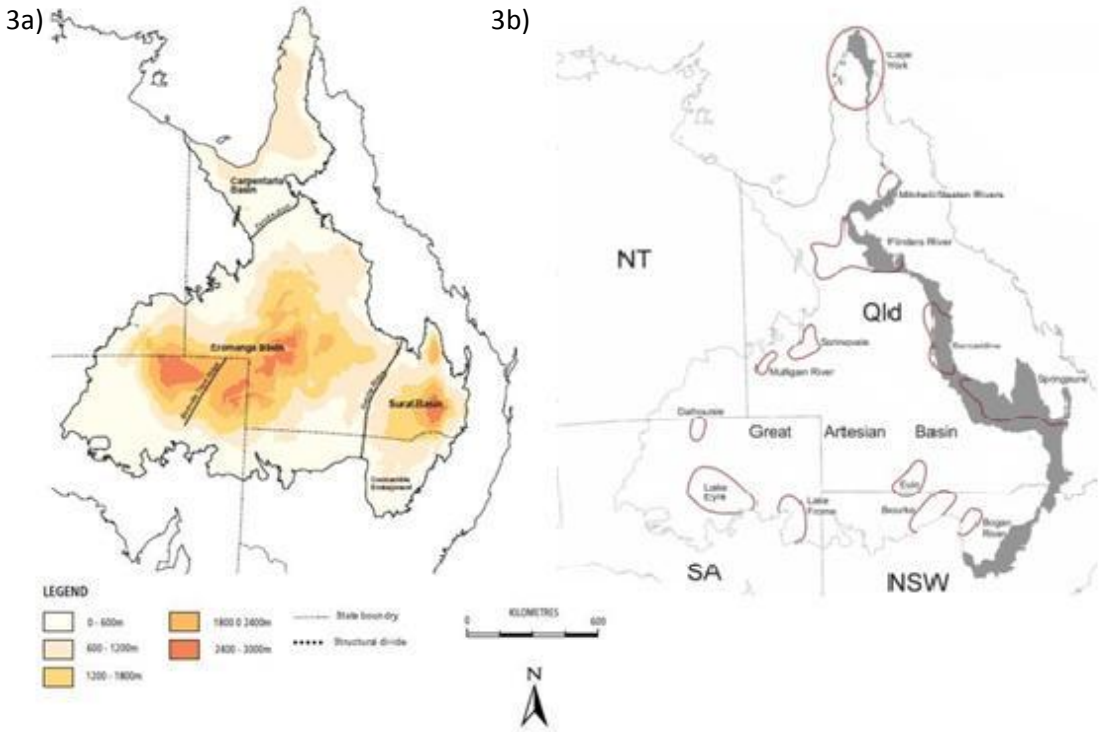

Figure 4a & 4b

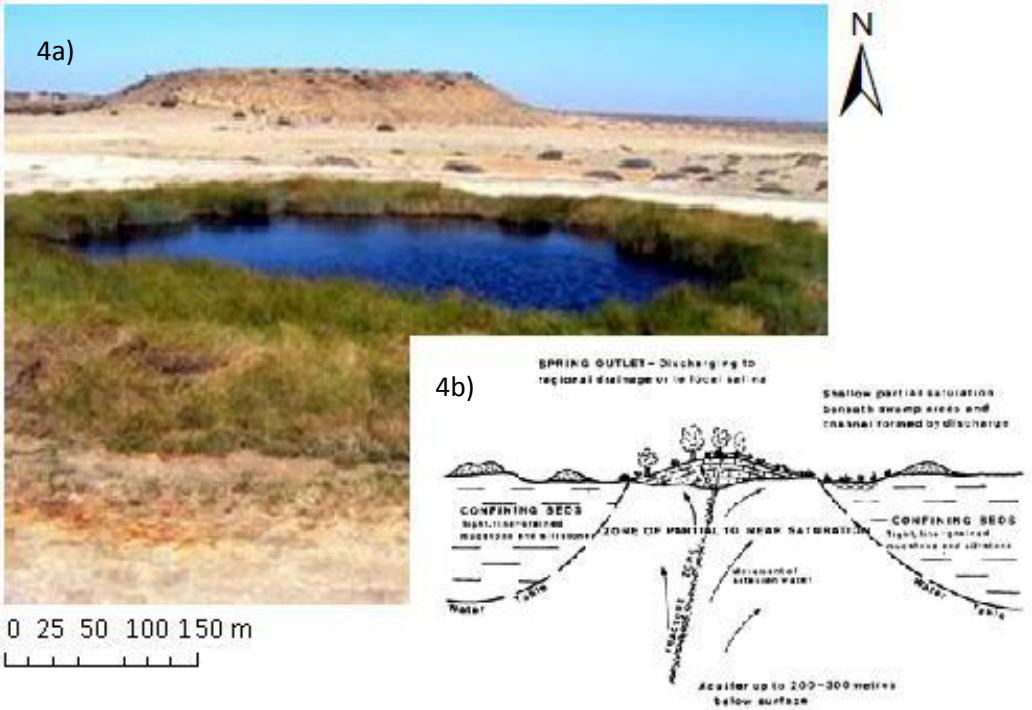

Figure 5

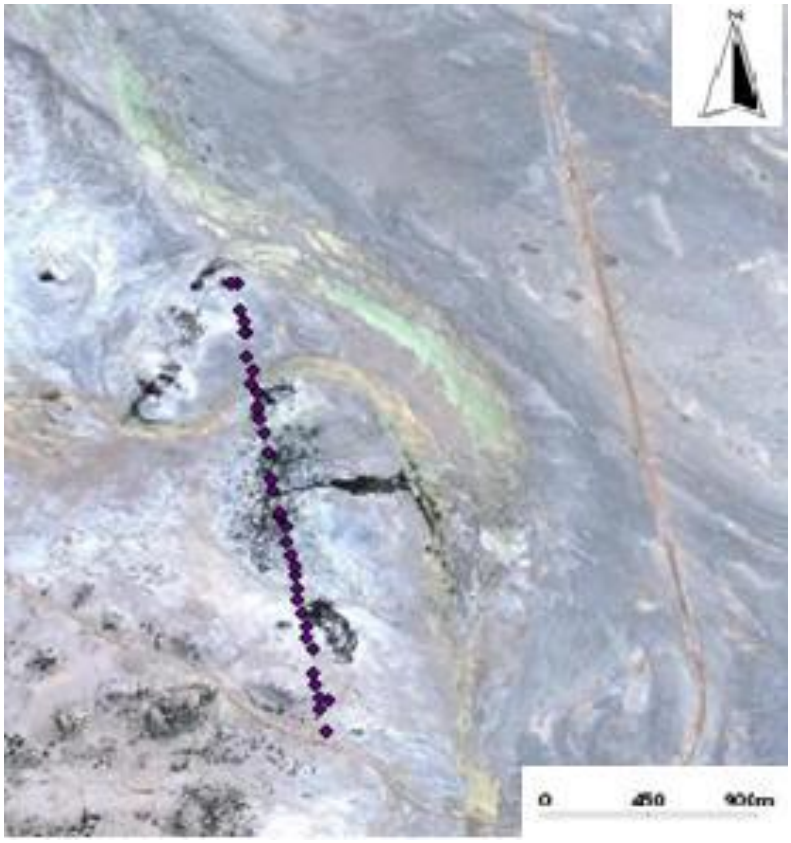

Figure 6

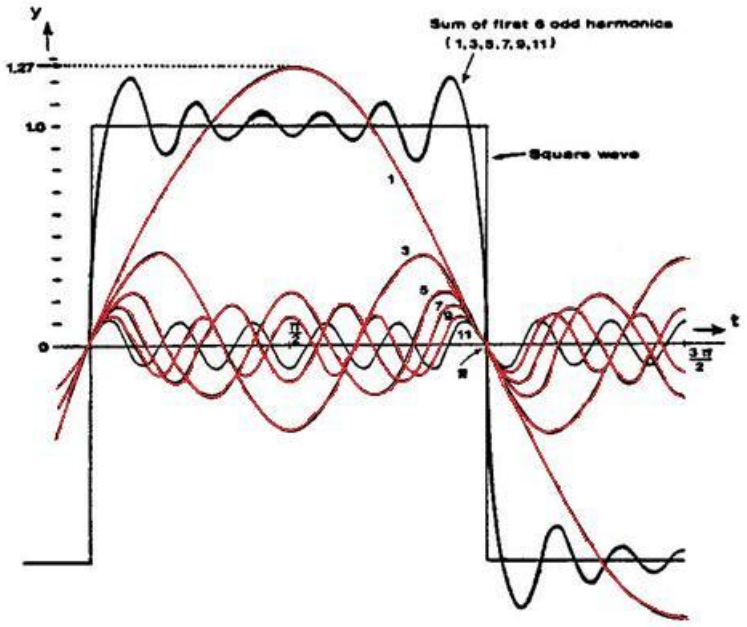

Figure 7a & 7b

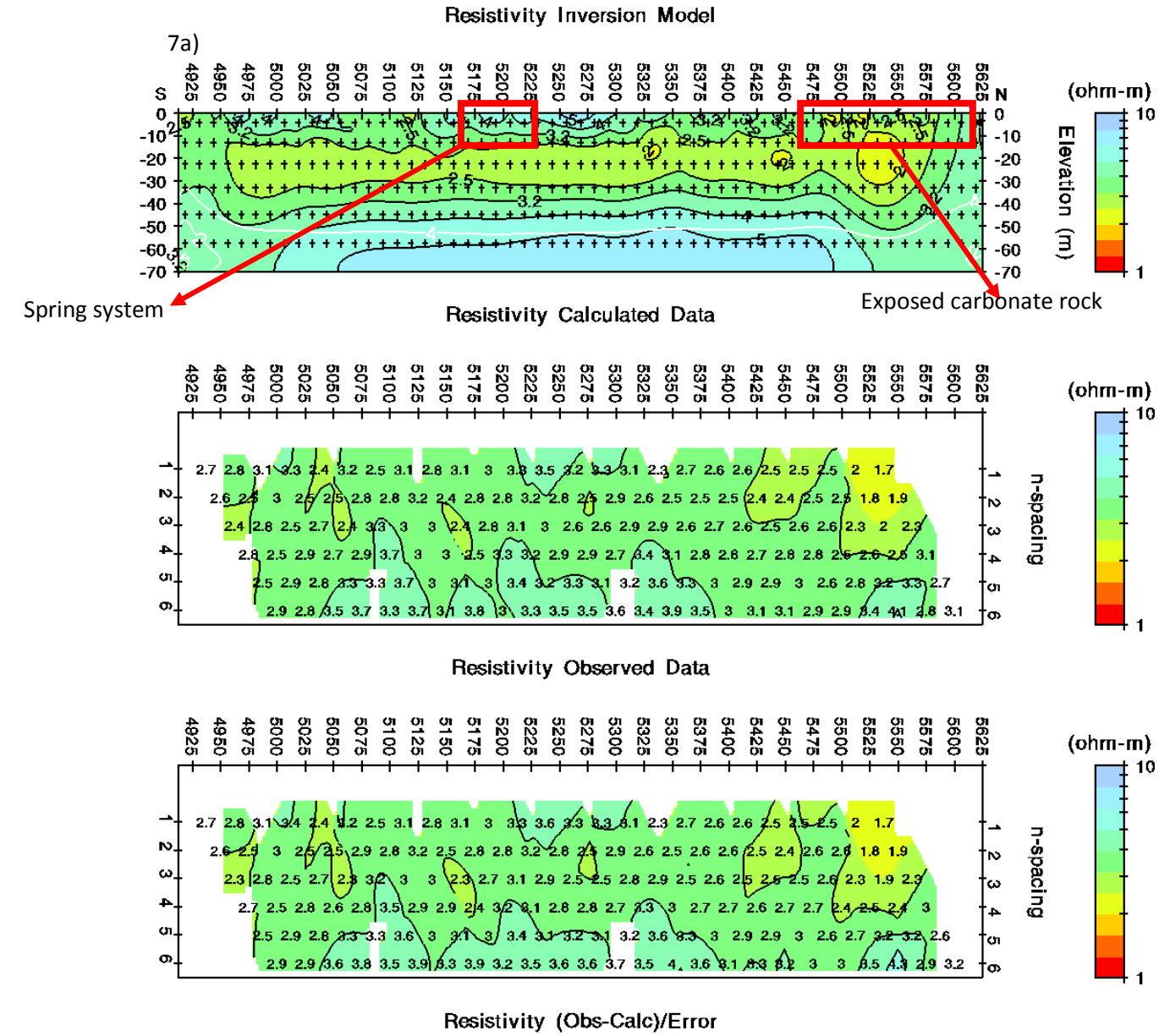
Resistivity Inversion Model
7a)
S
N
Elevation (m)
(ohm-m)
Spring system
Exposed carbonate rock
Resistivity Calculated Data
Resistivity Observed Data
Resistivity (Obs-Calc)/Error
n-spacing

7b)

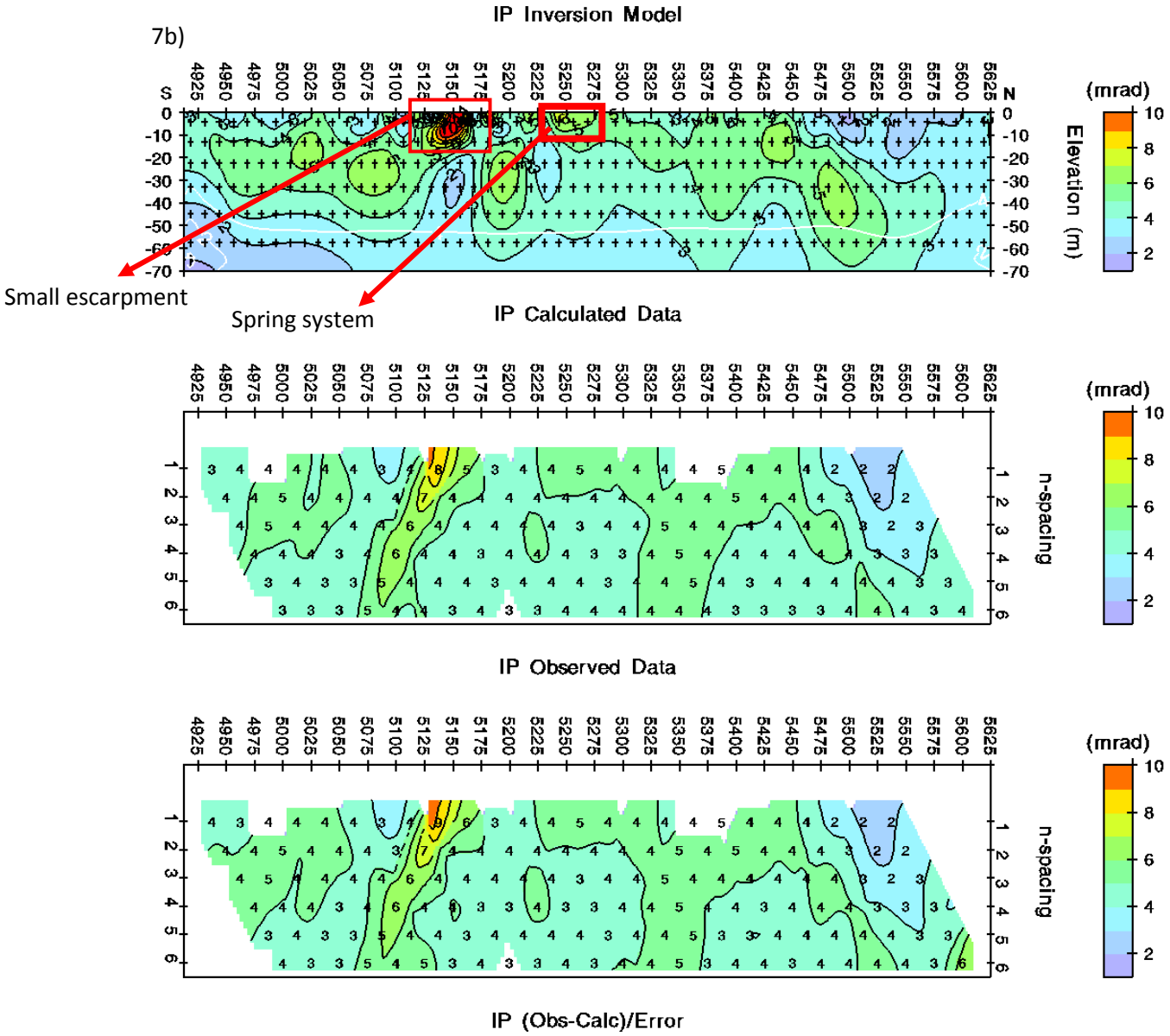
IP Inversion Model
S
N
Elevation (m)
(mrad)
Small escarpment
Spring system
IP Calculated Data
n-spacing
IP Observed Data
IP (Obs-Calc)/Error

Figure 8a, 8b & 8c

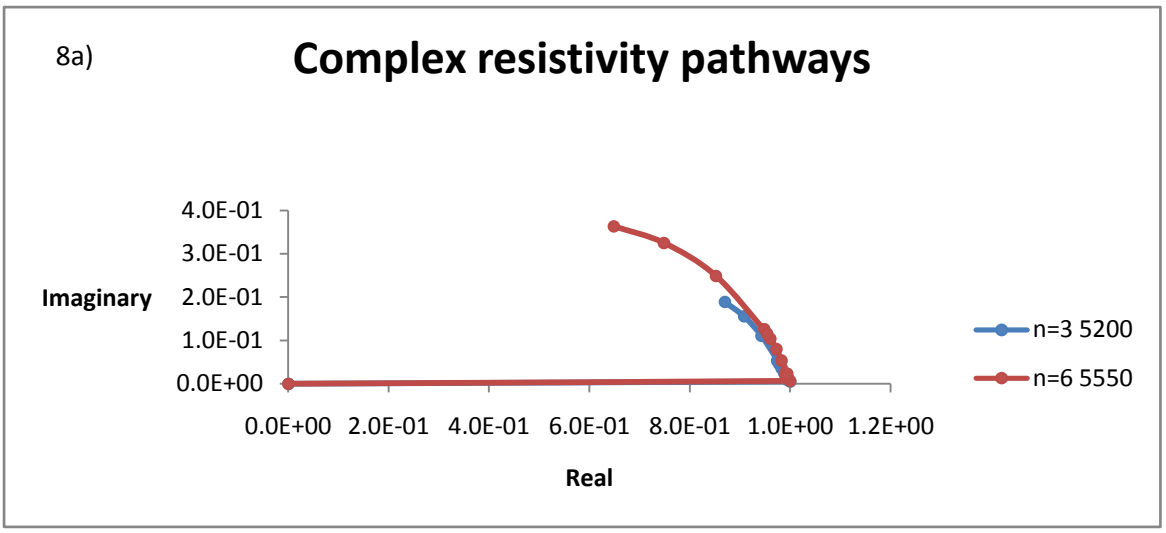

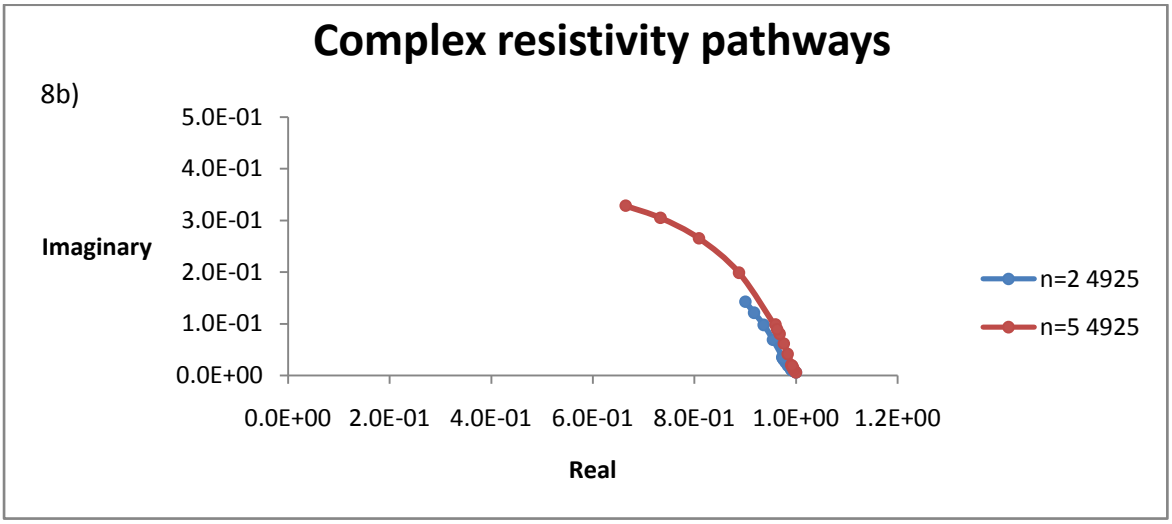

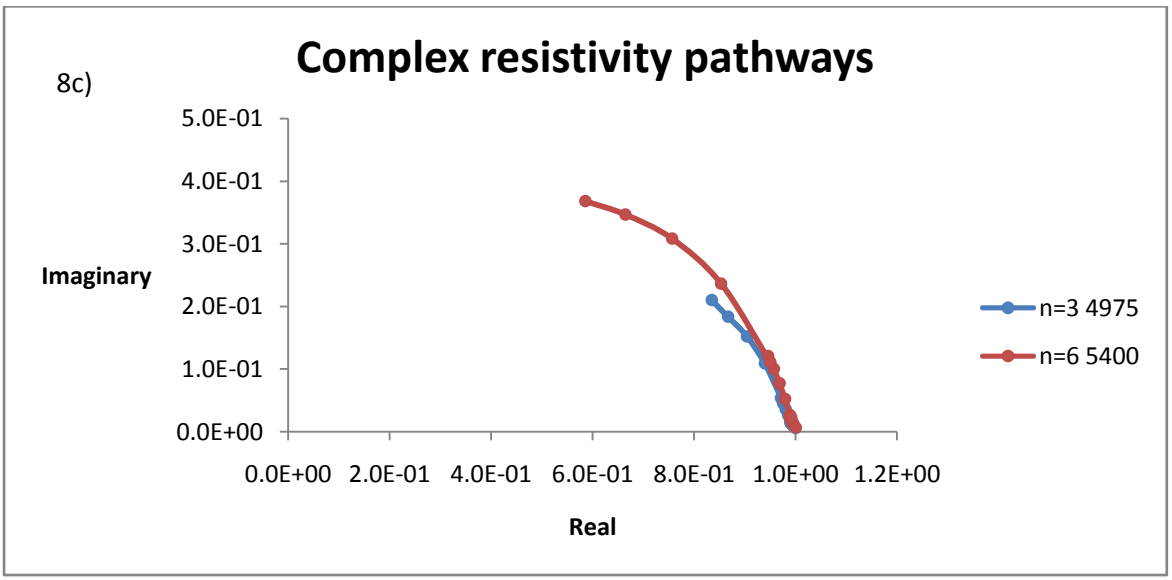

Figure 9a & 9b

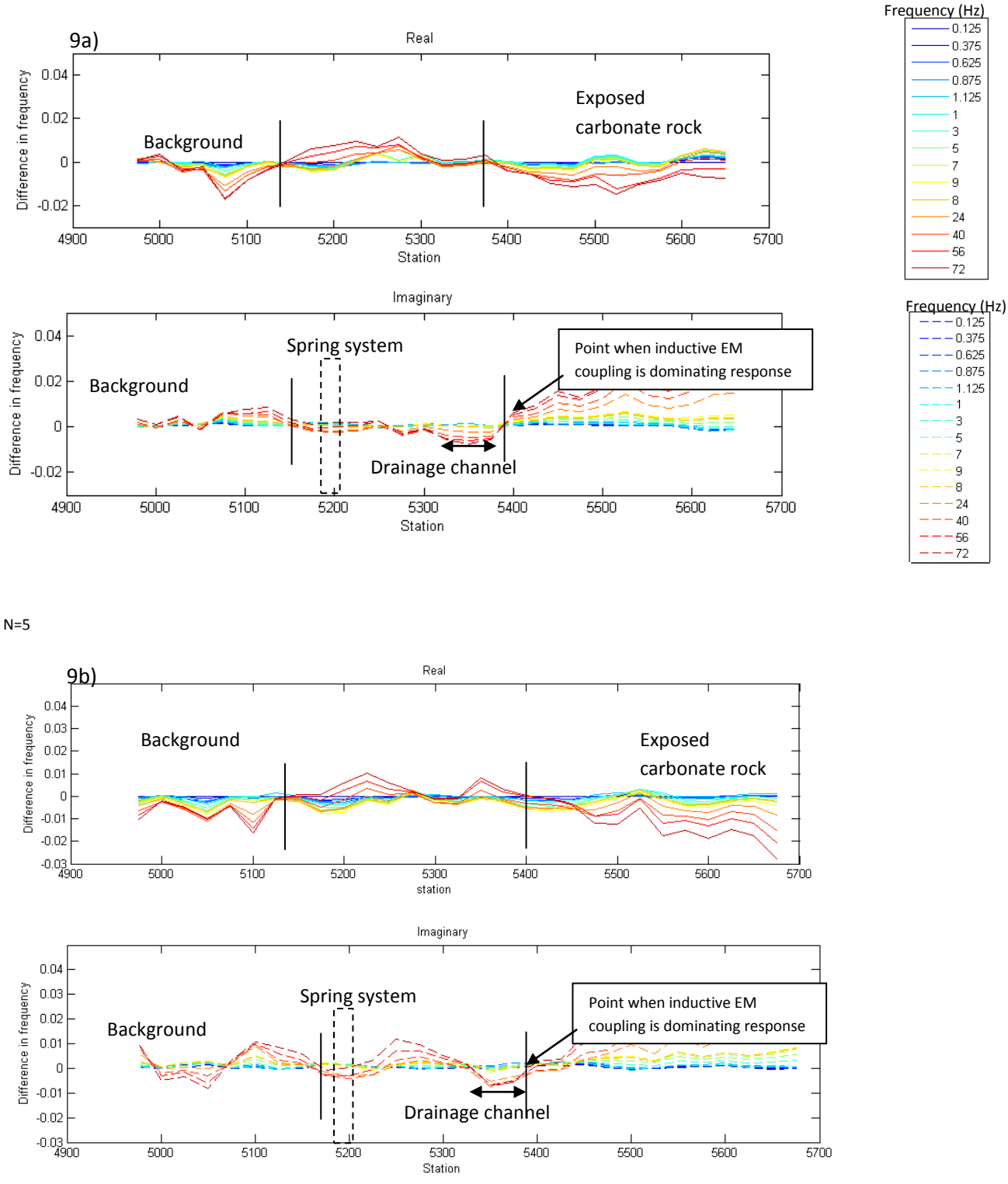
N=3
9a)
Real
Difference in frequency
Background
Exposed
carbonate rock
Station
Frequency (Hz)
0.125
0.375
0.625
0.875
1.125
1
3
5
7
9
8
24
40
56
72
Imaginary
Spring system
Point when inductive EM
coupling is dominating response
Background
Drainage channel
Station
N=5
9b)
Real
Background
Exposed
carbonate rock
station
Imaginary
Spring system
Point when inductive EM
coupling is dominating response
Background
Drainage channel
Station

Figure 10a & 10b

n=3

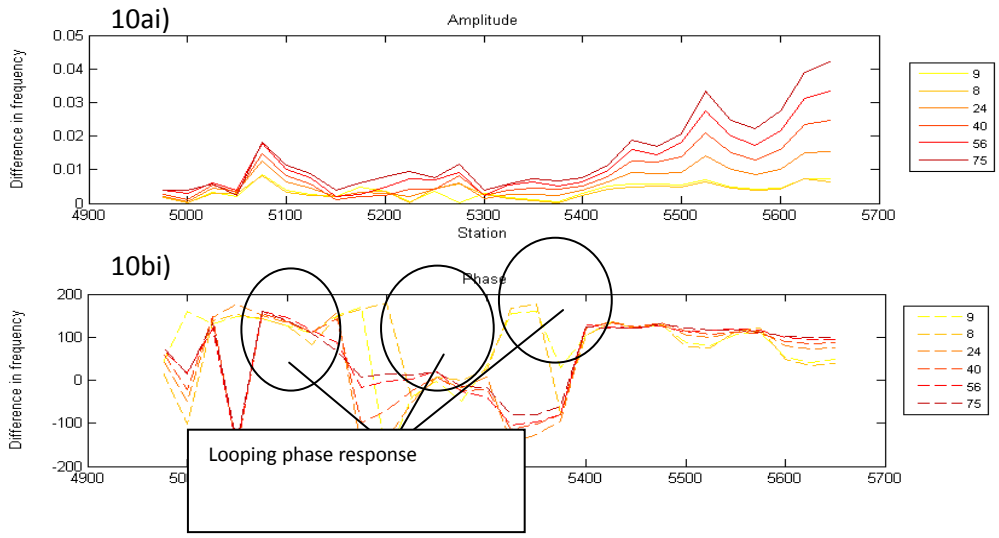

n=5

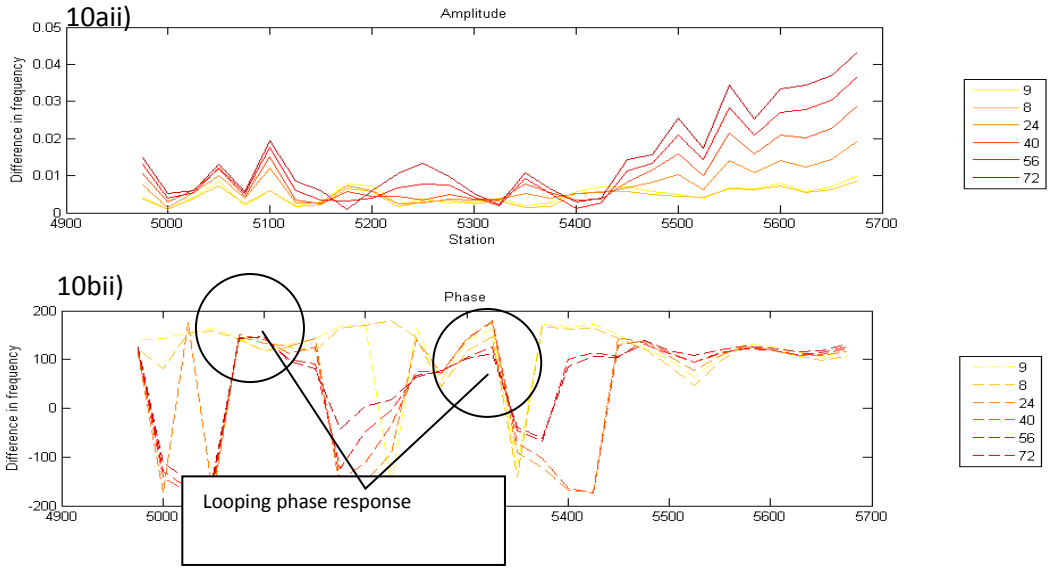

Figure 11a & 11b

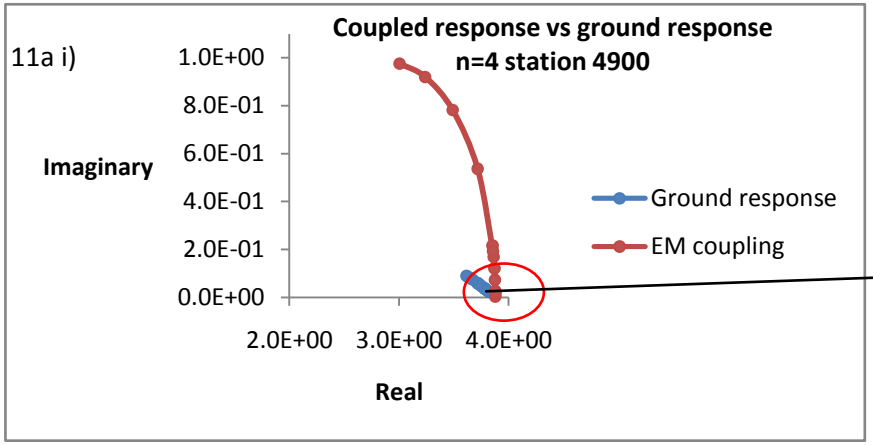

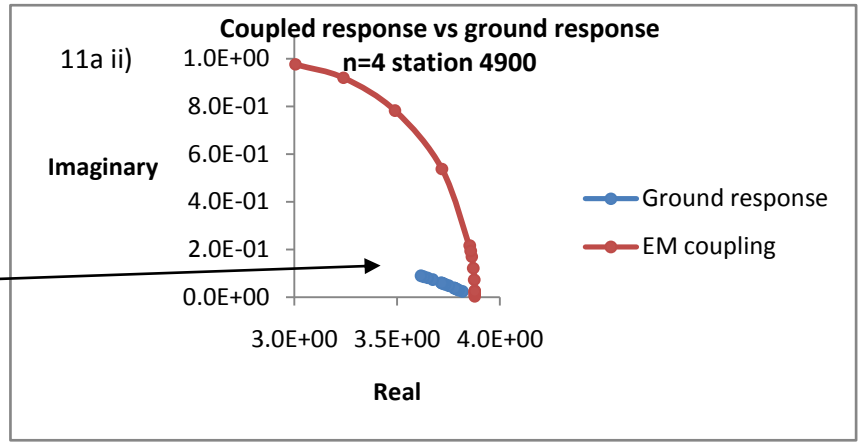

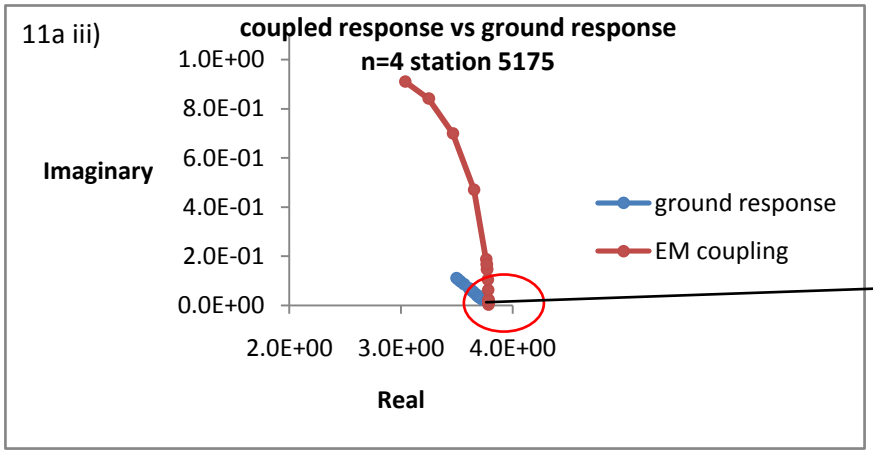

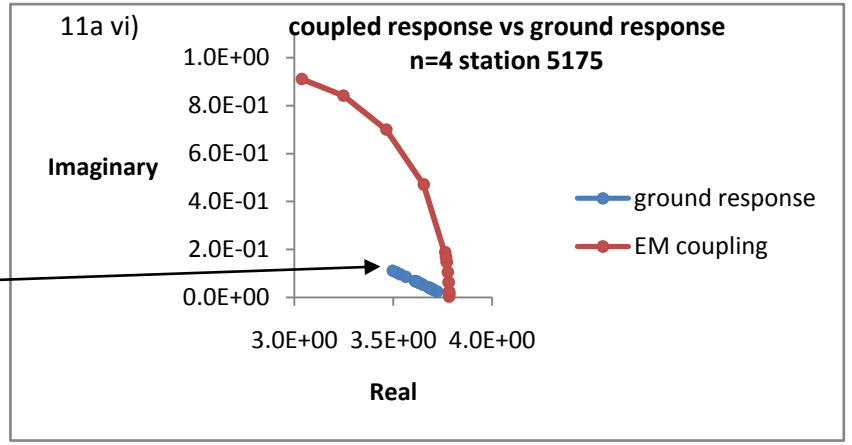

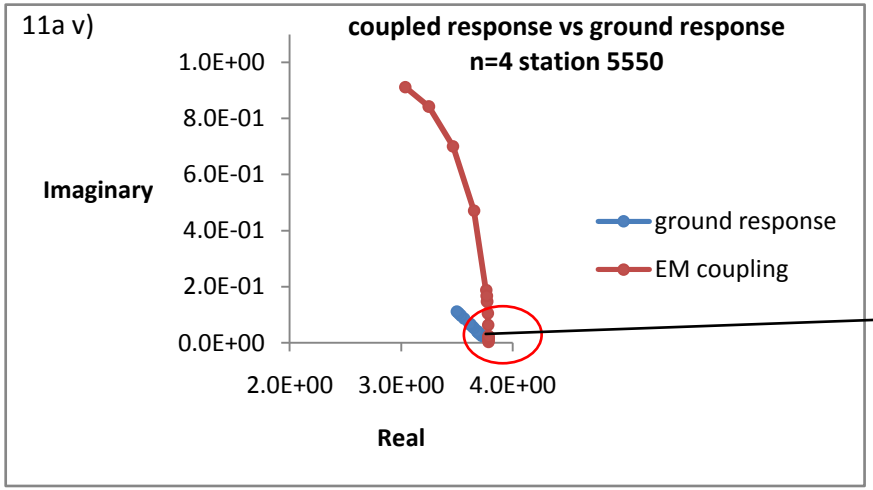

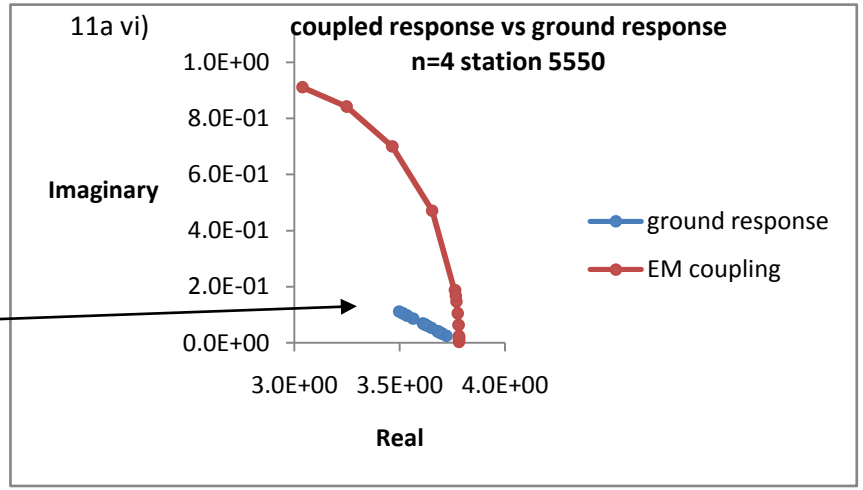

11b i)

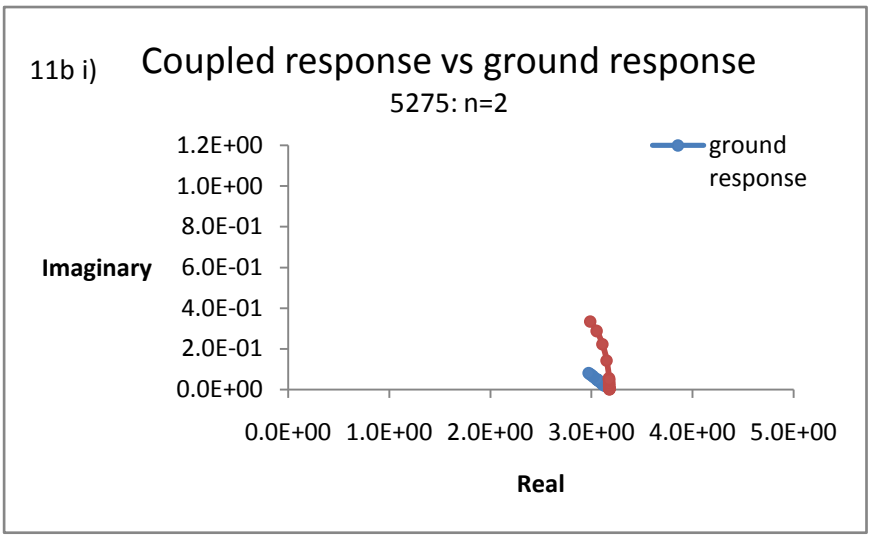

11b ii)

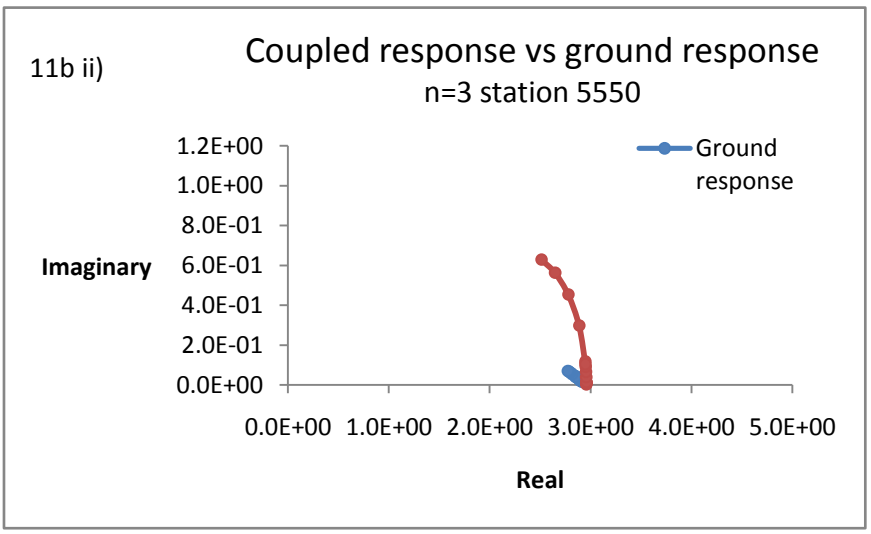

11b iii)

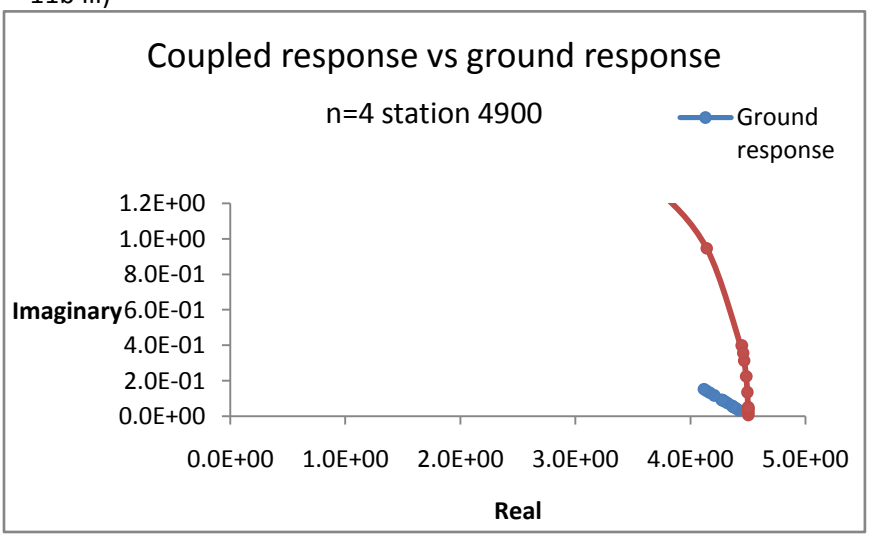

Figure 12

12a)

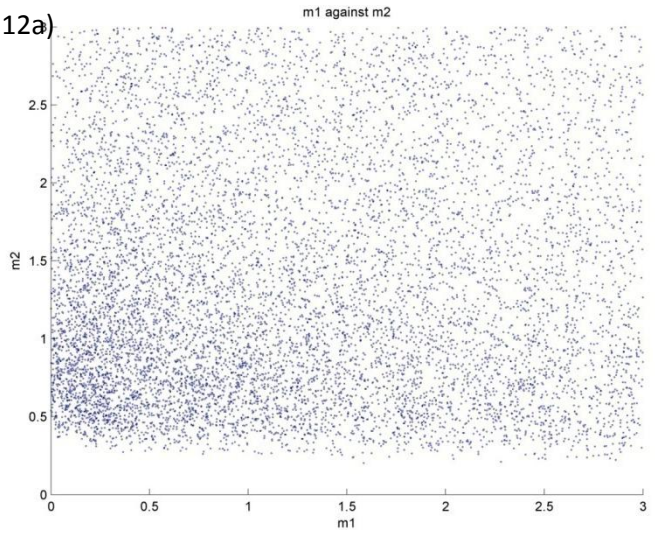

12b)

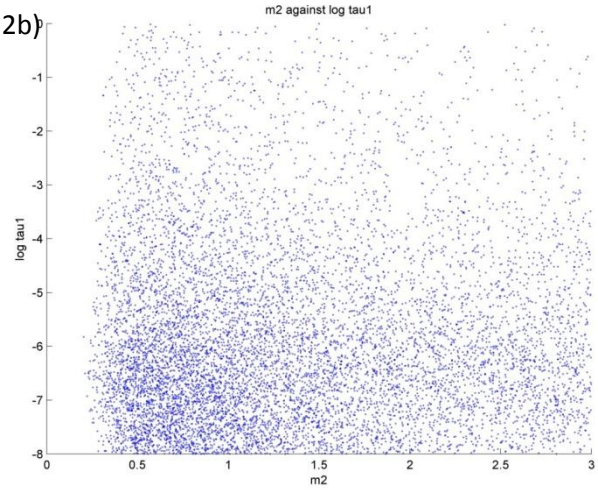

12c)

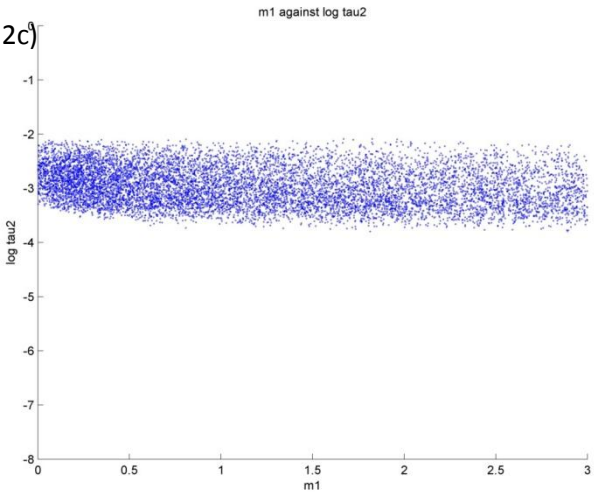

12d)

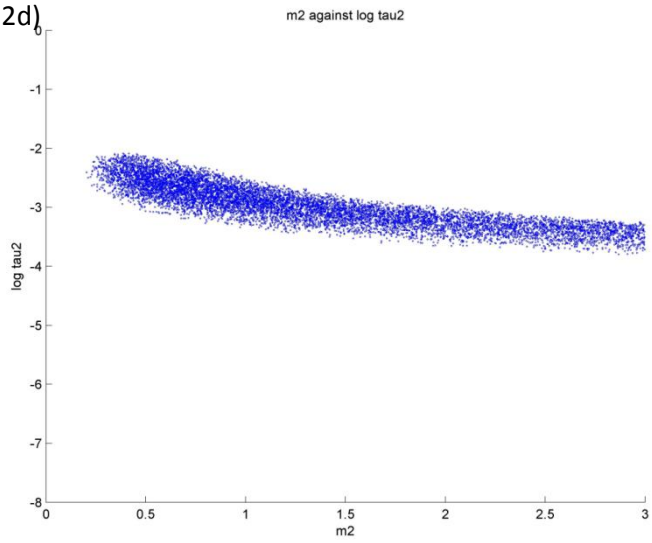

12e)

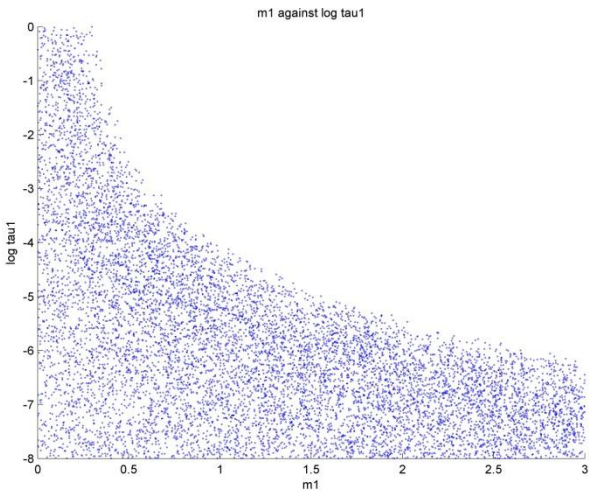

Figure 13

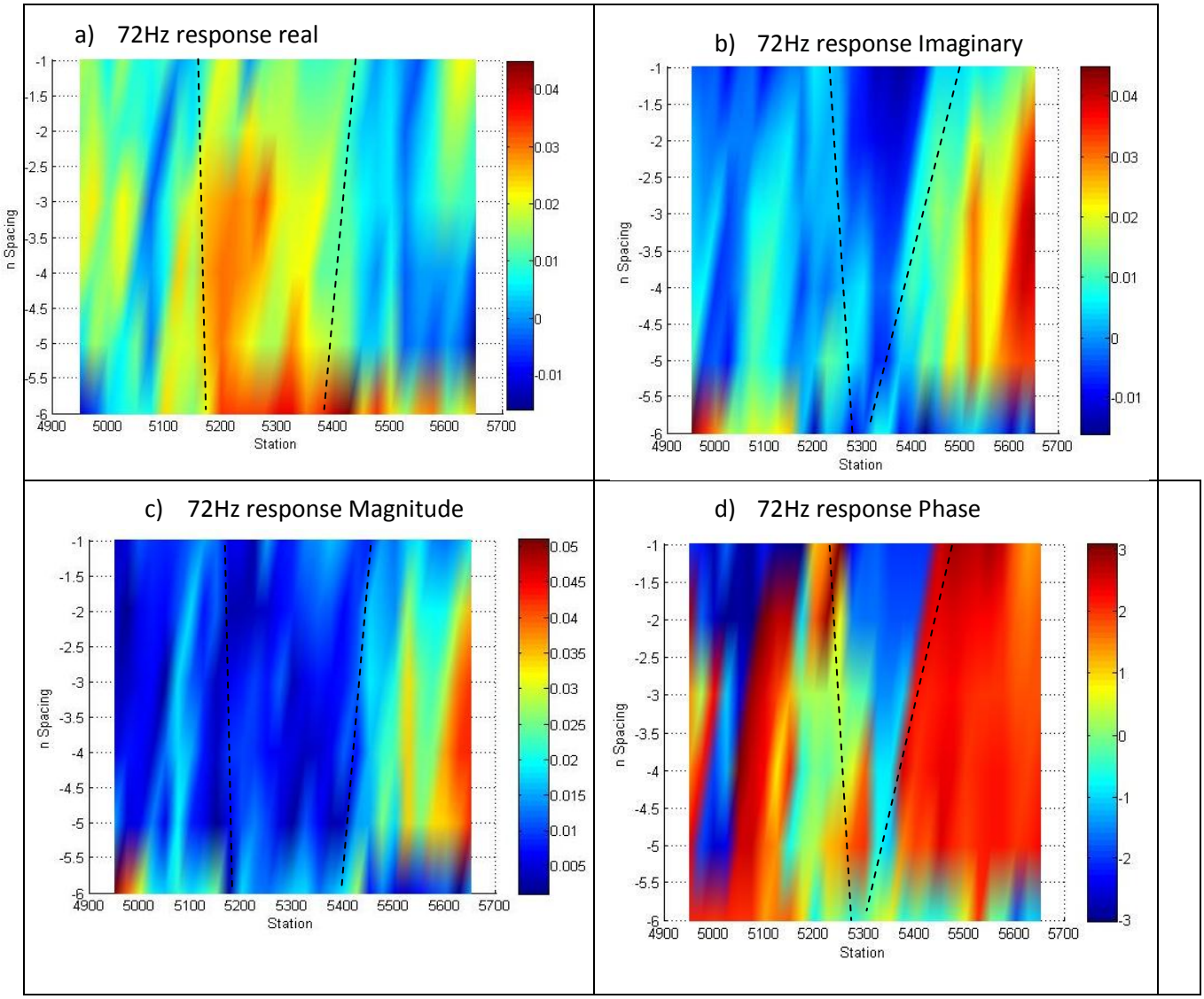
a) 72Hz response real
b) 72Hz response Imaginary
c) 72Hz response Magnitude
d) 72Hz response Phase
n Spacing
Station

Figure 14

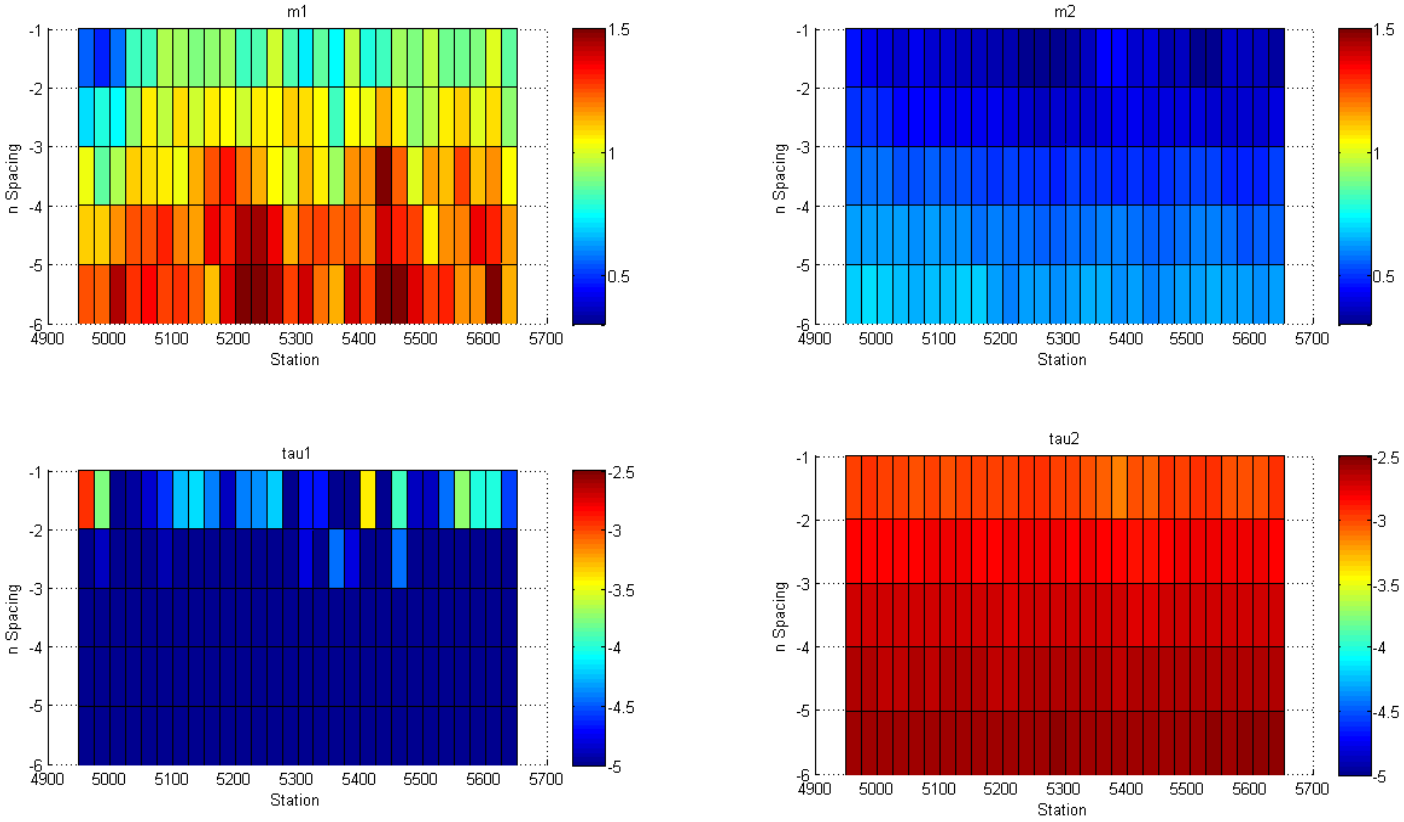
m1
n Spacing
Station
-1
-2
-3
-4
-5
-6
4900
5000
5100
5200
5300
5400
5500
5600
5700
1.5
1
0.5
m2
n Spacing
Station
tau1
n Spacing
Station
-2.5
-3
-3.5
-4
-4.5
-5
tau2
n Spacing
Station

11.0 Appendix

Raw data

See attached document